Compact folded-shorted patch array offering dual-band operation and dual-circularly polarized radiation for picosatellites and other small satellites

Compact folded-shorted patch array offering dual-band operation and dual-circularly polarized radiation for picosatellites and other small satellites

Bandar Alshammari,[1,2] Khalid M. Alrushud,[1,2] Yuepei Li,[3,1] and Symon K. Podilchak[1,3,✉] (iD)

[1]*Institute for Imaging, Data and Communications (IDCOM), The University of Edinburgh, Edinburgh, Scotland UK*

[2]*King Abdualaziz City for Science and Technology (KACST), Riyadh, Saudi Arabia*

[3]*Institute of Sensors, Signals, and Systems, Heriot-Watt University, Edinburgh, Scotland UK*

✉ Email: s.podilchak@ed.ac.uk

Fig. 1 *Proposed 2×2 folded-shorted patch (FSP) array prototype for proof-of-concept by sequentially rotating four linearly polarized elements. The dual-band antenna structure is fed by 8-ports and this can support dual-circularly polarized (DCP) radiation. The major dimension of the array corresponds to 5 cm, or 0.18λ at the lower operational frequency of the antenna (which is contained within the L-band)*

The development of a dual-band folded shorted patch (FSP) antenna array is presented which offers dual-circularly polarized radiation. Applications include small satellites like CubeSats and picosatellites. The proposed 2×2 FSP array design operates at 1.1 and 2.4 GHz and offers good radiation performance in terms of minimal reflection coefficient losses, broad beamwidths (which is generally required for low gain antenna structures ensuring link connectivity), as well as low cross-polarization levels. The antenna array consists of a meandered layer defining the top of the FSPs. The shorting and folding technique as well as the noted meandering allows further size reduction of the quarter-wavelength patch. In particular, the proposed antenna array is compact with a total size of 50 mm by 50 mm (or 0.18λ by 0.18λ at the lower operational frequency). An eight-port coaxial and microstrip feed system is integrated onto the backside of the antenna ground plane, two ports for each element, and with external phase feeding of $90°$, dual-circularly polarized is made possible for the compact antenna unit. To the best knowledge of the authors, no similar antenna structure has been designed, manufactured and tested being useful for picosatellites and other small satellites.

Introduction: Traditionally large-scale satellites have dominated the space sector with high costs, and being mainly developed by government agencies, militaries, and large companies [1, 2]. These conventional satellites have been used for broadcasting, telecommunications, navigation, remote sensing, and planetary observational research. In an effort to reduce costs, small satellites have become a popular research trend where the emphasis has been on reduced size and weight, and this has also been coupled with mass production, resulting in significant advancements in CubeSat research [3]. Moreover, these SmallSats (i.e. cube-satellites, pico-satellites, and micro-satellites), have become increasingly popular in recent years for use in low Earth orbit (LEO) applications new space research and for communications [3–6].

Antennas are one of the most important components of these SmallSats. They are mainly used for communicating with the ground station, high-speed data downlinks, inter-satellite communications etc. and therefore, the need for suitable antennas is vital to achieve these reduced cost and small volume constraints. In addition, these antennas need to meet several requirements, but the most important is the size limitation [7]. This is because the antenna size should be less than the 1U model (10 cm $\times$10 cm $\times$10 cm) for CubeSats and mountable on such platforms, and similarly, 5 cm $\times$5 cm $\times$5 cm for picosatellites [8].

Considering microstrip patch antennas (MPAs), they are favourable for such SmallSats due to their low profile and planar configurations, low cost, light weight, and suitability for array designs as well as simple integration and PCB fabrication [9–11]. Therefore, the common MPA is probably one of the best options for SmallSats and major dimensional sizes are about $\lambda/2$ (where λ is the free-space wavelength for the antenna operating frequency). However, implementing this kind of antenna on the surface of CubeSats and picosatellites might be very difficult due to the aforementioned size limitations. To meet these requirements, the resonant antenna length can be further reduced to $\lambda/4$ (and more) by introducing a shorting wall and ground plane folding [8, 12, 13]. Efforts have also been made to further reduce the footprint of these folded-shorted
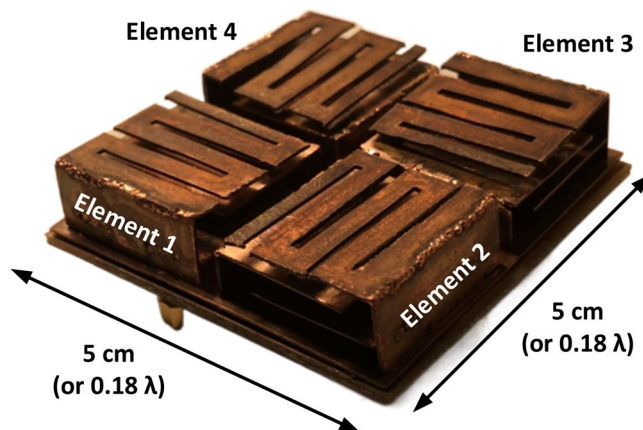
patches (FSPs), making them more suitable for CubeSat integration [8, 14–16]. The reason that these kinds of antennas are applicable and attractive for small satellites is that they are non-deployable whilst being low profile and generally have reduced manufacturing costs. Also, these antennas have been designed at UHF and L-band frequencies for SmallSats [8, 13, 14] such as the Unicorn PicoSat series by Alba Orbital [17] and the Maritime Monitoring and Messaging Microsatellite (M3MSat) mission for the Canadian Space Agency [18].

In an effort to advance upon these earlier developments, we propose herein a dual-frequency and dual-circular polarization (DCP) array design using four FSP antenna elements (see Figure 1). In particular, this work follows previous efforts reported in [8] and [13] where the proposed DCP antenna structure (in this letter, and for proof-of-concept) similarly employs meandering of the top layer as well as folding and shorting techniques for the metallic antenna elements to enable compactness, but however, has been newly optimized for dual-frequency operation; i.e. by controlled radiation of the TM_{010} and the TM_{030} modes of the FSPs. Moreover, it should be made clear that the 4-port antenna designs in [8] and [13] only offered single-band operation and one circular polarization (CP) state, where as the structure in this letter offers DCP, as well as, dual-band operation. To achieve this DCP, the proposed antenna was designed with 8 feed points and with a small size of 5 cm by 5 cm, making it applicable for picosatellites. A comparison of the newly reported and manufactured design is outlined in Table 1 as well as other relevant antenna structures found in the literature. As it can be observed, and to the best knowledge of the authors, no similar compact antenna structure offers dual-band and DCP functionality.

As further discussed in the following, the proposed 2×2 FSP antenna array was optimized for dual-band operation at about 1.1 and 2.4 GHz, i.e. the L-band and S-band, respectively. These dual-band frequencies can be selected by the appropriate dimensions of the folded patch and shorting walls, spaces between the layers, and the meandered top layer of the antenna structure. Furthermore, the proposed design achieves DCP by introducing two feed points for each linearly polarized FSP single-element, which is then sequentially rotated in a 2×2 array arrangement for CP radiation (see Figures 1–3). This antenna structure requires external feeding for its eight ports, but it can be easily integrated on one surface of a PicoSat, for example, as the major antenna size (i.e. length and width) is only 50 mm by 50 mm.

The proposed dual-band and DCP antenna can support S-band downlinks and multiple transmitting and receiving functions for communications and positioning as well as data links between more larger-scale satellites (which typically operate at the L-band) within a single array structure. Furthermore, the design also has the functionality to enable communications between a network of CubeSats (enabling satellite-to-satellite connectivity) or ground station communications [22], for example, while also, not consuming excessive area on the satellite structure

Table 1. Comparison of the proposed design to other similar antennas reported in the literature

Work	Antenna type	Number of layers	Number of elements	Design frequency	Reflection Coefficient	Antenna or array size	Dual band	Dual CP
[8]	Metallic	2	2×2 Array	1.1 GHz	-15 dB	$0.18\lambda \times 0.18\lambda$	No	No
[13]	Metallic	4	2×2 Array	0.400 GHz	< -10 dB	$0.20\lambda \times 0.20\lambda$	No	No
[15]	Metallic	2	2×2 Array	0.400 GHz	-34 dB	$0.67\lambda \times 0.67\lambda$	No	No
[19]	Metallic	4	Single element	0.415 GHz	-13 dB	$0.28\lambda \times 0.28\lambda$	No	No
[20]	Metallic & PCB	2	Single element	2.4 GHz & 5 GHz	-28 & -29 dB	$0.30\lambda \times 0.30\lambda$	Yes	No
[21]	Metallic	2	Single element	0.84 GHz	-26dB	$0.56\lambda \times 0.56\lambda$	No	No
This Work	Metallic	3	2×2 Array	1.1 GHz & 2.4 GHz	-12 dB & -15 dB	$0.18\lambda \times 0.18\lambda$	Yes	Yes

Note: where λ is the free-space wavelength at the lowest design frequency.
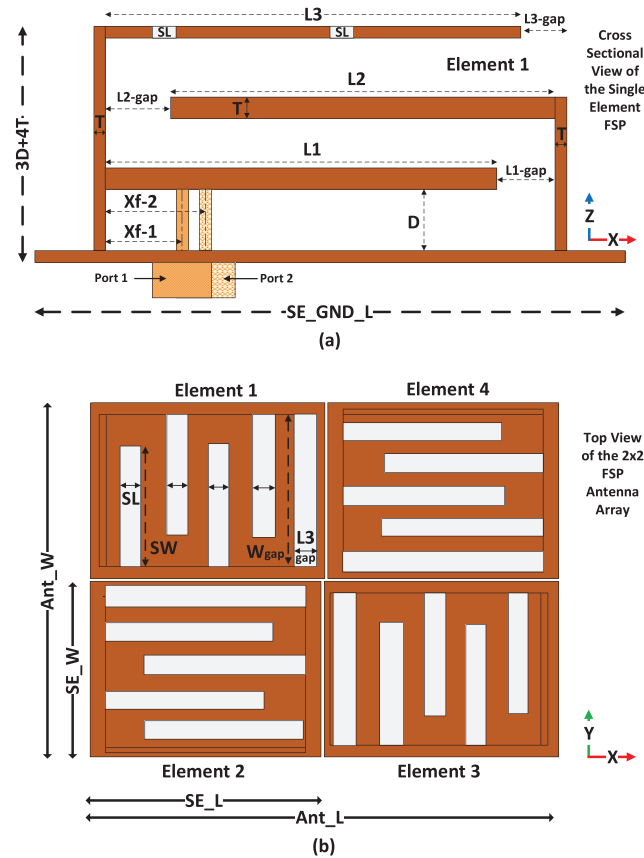

Fig. 2 *(a) Cross-sectional view of Element 1 within the 2×2 FSP antenna array, and (b), top view of the array where the top layer meandering is shown (see dimensions in Table 2)*

Fig. 3 *Bottom view for the fabricated 2×2 FSP antenna array where the 8 connecting ports are shown and defined as P1 to P8. Element 1 is connected to ports 1 and 5 using two probes, two gold leaf filaments, two 50-Ω microstrip lines, and, two SMP connectors (similarly for elements 2–4). This arrangement supports connectivity to external feeding circuits or one which can be mounted on the bottom side enabling DCP operation*

itself. This leaves more space on the PicoSatellite for other devices, sensors, solar panels, and deployable systems etc. and this enhances the possible space mission capabilities.

Overview and antenna design approach: It should be mentioned that some preliminary findings of an earlier version of the proposed FSP antenna array were originally reported in [23]. Simulation results showed that the antenna can work at 1.1 and 2.1 GHz. In this letter, we further optimise the 2×2 FSP antenna array for slightly different operating frequencies, mainly, at 1.1 (L-band) and 2.4 GHz (S-band). This is because 2.4 GHz is more typically required for downlinks [22] and inter-satellite data-links. In addition, in this letter, this newly proposed and further optimized structure, has been fabricated and experimentally tested for proof-of-concept.

It should be mentioned that other previous works have also studied DCP and dual-band FSPs, but not both. For example, in [20], a 0.3λ by 0.3λ single-element structure was reported for dual-band operation using a printed PCB for the top-layer. Another work, [15], studied the use of two array of FSPs for CubeSats offering DCP by using sequential
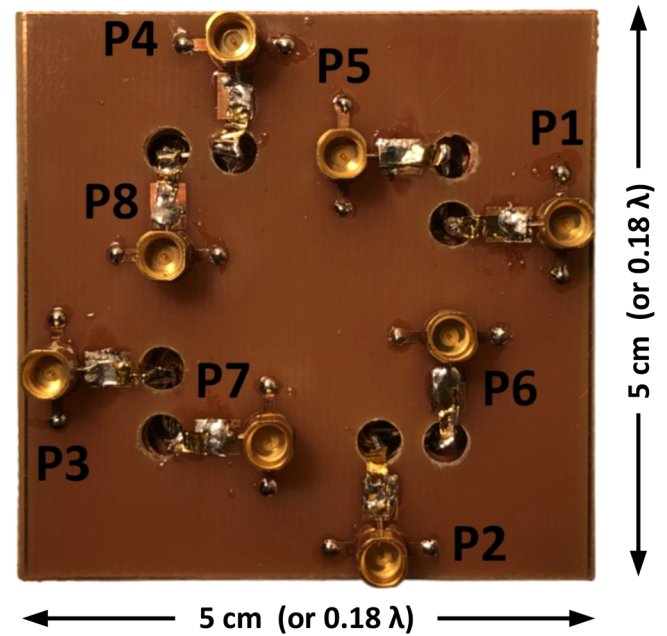
rotation. Moreover, the two spatially separated antenna arrays in [15] were designed and positioned on two opposite surfaces of the satellite structure in that eight radiating elements were required (4 for each array, for an antenna size of 0.67λ by 0.67λ). To further highlight the benefits of our proposed single-unit antenna design, it is more compact (0.18λ by 0.18λ) and uses only four FSP elements for the 2×2 array (not eight as in [15]), whilst also, offering dual-band operation and DCP functionality.

Single-element folded shorted patch design: The proposed antenna unit was firstly designed as a single-element following previous efforts as in [12, 19–21]. See also Table 1 where it shows the previous developments for other single elements and 2×2 FSP antenna arrays which offer single-band and individual CP radiation only. Basically, the folding and shorting technique was introduced for the proposed antenna as well as the meandering of the top layer. This reduced the physical size and enabled overall structure compactness for picosatellite integration.

The four single element antennas all have the same dimensions, and each single element is further defined in Table 2. Also, the length and width of the ground plane for each single element is described as SE_GND_L and SE_GND_W. Also, the single-element structure consists of three layers and all of them have the same major width of W, but different lengths for layer 1, layer 2, and the meandered layer 3 (L1, L2, and L3). The spacing between the layers is D. In addition, the distance between the three layers and the walls is de-

Table 2. Dimension for the proposed 2×2 FSP antenna array

L1	L2	L3	W	T	D
16 mm	17 mm	19 mm	22 mm	0.5 mm	2.5 mm
L1_gap	L2_gap	L3_gap	SL	SW	W_gap
5.5 mm	4.5 mm	3 mm	1 mm	17.5 mm	22 mm
Xf_1	Xf_2	SE_W	SE_L	SE_GND_L	SE_GND_W
9.8 mm	9.8 mm	22 mm	22 mm	25 mm	25 mm

fined as L1_gap, L2_gap, and L3_gap. Also, the width of the gaps between the layers and walls (W_gap) is the same as W. Furthermore, the manufactured antenna structure is defined by copper with a thickness of T.

Each single-element was fed by two coaxial probes and microstrip feedlines optimized for 50-Ω matching and were positioned in the bottom side of the ground plane. These microstrip lines were connected to SMP surface mount connectors. The probes were located at a distance of (XF_1 and XF_2) from the shorting wall (see Figure 2). The top meandered layer, has four slots that have a length and width of SL and SW. All the dimensions (see Table 2) for the four single-element FSP antennas were originally optimized in order to adjust the operational lower and upper frequencies to about 1.1 and 2.4 GHz, respectively.

Folded-shorted patch antenna array: The proposed 2×2 compact FSP antenna array is dual-band and can achieve DCP, and the complete structure was further optimized after the aforementioned single-elements were positioned within the array. As shown in Figure 2, the structure is made of four single-element antennas (elements 1–4). The total antenna array dimensions are 50 mm $\times$ 50 mm, being suitable for picosatellites and other CubeSats whilst meeting the size limitations for these small satellites. The four elements are all linearly polarized (LPs), and by using sequential rotation, DCP is possible for the eight-port antenna as well as other polarization states enabling diversity [24, 25]. CST simulations of the reflection coefficients for Element 1 are reported in Figures 6 and 7 for the optimized structure at the lower and upper operating bands, respectively.

In this 2×2 FSP array, each single-element has two different 50-Ω feed points. This enables the FSP elements to offer two different linearly polarized (LP) operating states. Moreover, the 2×2 FSP antenna array can be made to offer DCP, mainly, by using the noted sequential rotation technique and with equal amplitude and sequential phase shift either by $90°$ or $-90°$ at the ports. Given that the FSP array has a total of eight coaxial feed probes, they can be described as ports 1–8 (see Figure 3). To enable DCP for the antenna structure, these eight ports have been distributed between all four elements (i.e. two ports for each single-element, see Figure 3).

Ports 1, 2, 3 and 4 dictate the first CP antenna state and we define this as circular polarization 1 (CP1). And the other ports, 5–8, relate to circular polarization 2 (CP2). While each antenna element has to have a specific phase advance/delay of $0°$, $-90°$, $-180°$, $-270°$ defining the right-handed circular polarization (RHCP) state, and $0°$, $+90°$, $+180°$, $+270°$ for the left-handed circular polarization (LHCP) state, we respectively define these two antenna operating states as CP1 and CP2, for simplicity. The corresponding electric field (magnitude and vector orientation) is reported in Figures 4 and 5 for different RHCP and LHCP cases. For both these simulations, the physical size of the FSP array and the radiating fields with respect to the free-space wavelength can be observed. These help to illustrate the orientation of the radiating fields and the general compactness of the antenna structure. In addition, to further document the CP radiating states, other field animations are also provided within the Supporting Information section for this letter.

Figure 8 also reports the realized antenna gain as a function of frequency for CP1 for the optimized design, and very similar findings were observed for CP2 (all results not reported for brevity) due to the symmetry of the structure. Other feeding configurations and polarization states are possible for the 8-port structure such as dual-linear and DCP when antenna diversity is of interest, similar to [24] and [25].
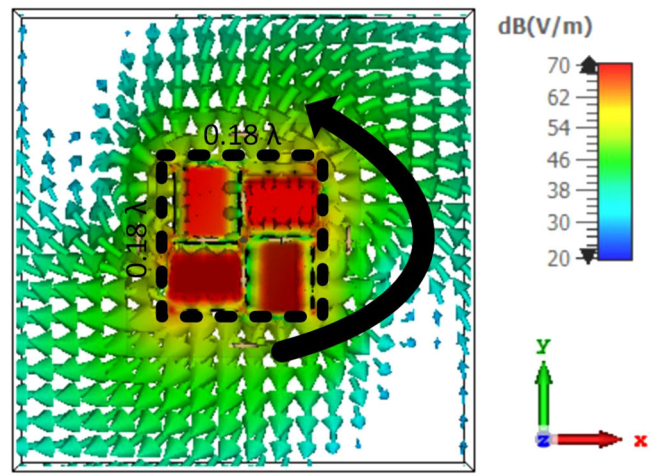

Fig. 4 The simulated E-field at the lower band for CP1 (RHCP), within a horizontal plane (3D/2 + 2T) defined in the middle of the 2×2 FSP array as well as an area surrounding the structure. Similar results were observed for CP2. The physical size of the antenna is outlined with a dashed line (and sized $0.180\lambda \times 0.18\lambda$, given the lower band operating frequency)
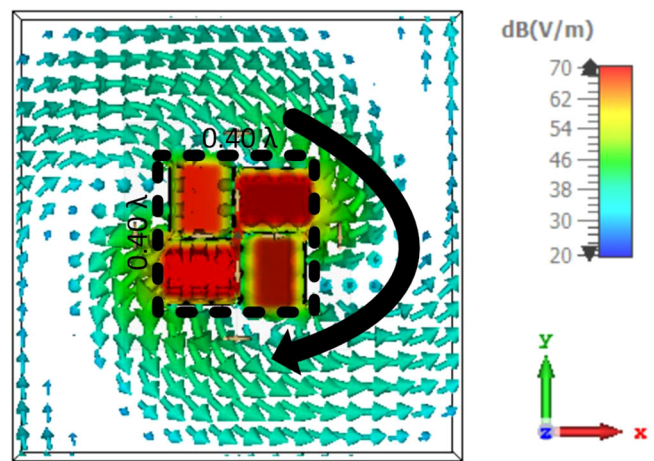

Fig. 5 The simulated E-field at the upper band for CP2 (LHCP), within a horizontal plane (3D/2 + 2T) defined in the middle of the 2×2 FSP array as well as an area surrounding the structure. Similar results were observed for CP1. The physical size of the antenna is outlined with a dashed line (and sized $0.40\lambda \times 0.40\lambda$, given the upper band operating frequency)
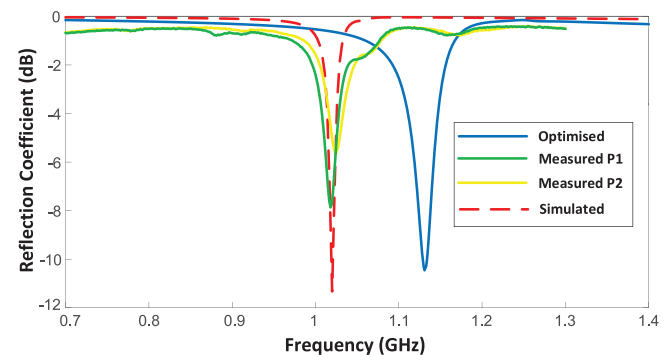

Fig. 6 Reflection coefficients for ports 1 and 2 at the lower band. Similar results were observed for the other ports (all results not reported for brevity)

Simulation results, array fabrication, and experimental testing: The dual-band and DCP 2×2 FSP antenna array was designed and simulated using CST. Results are reported in Figures 6–11 for the optimized design. Given these structure dimensions, the array was fabricated and assembled at The University of Edinburgh by the Mechanical and Electrical Technician Teams. In addition, the array was made out of copper with a thickness of 0.5 mm (see Table 2 for other relevant structure
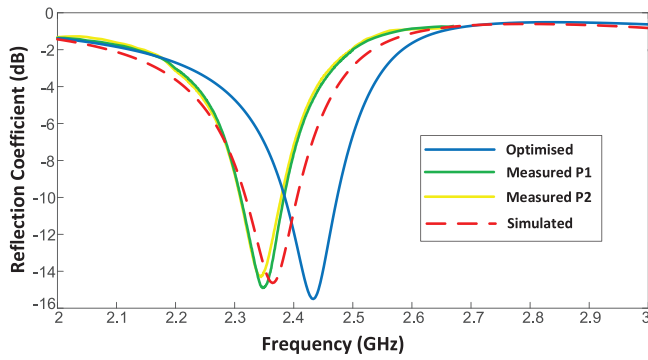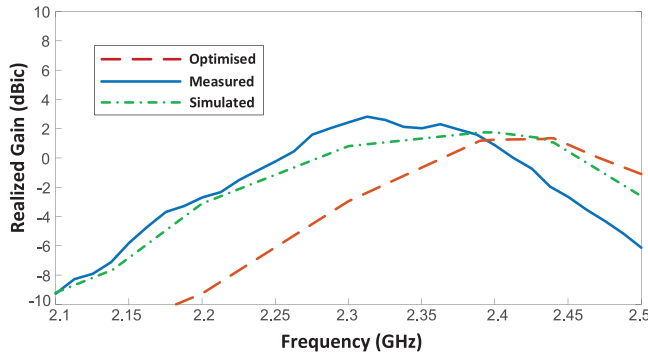
Fig. 7 *Reflection coefficients for ports 1 and 2 at the upper band. Similar results were observed for the other ports (all results not reported for brevity)*

Fig. 8 *Realized antenna gain (CP1) as a function of frequency for the 2 × 2 FSP array at the upper band. Similar results were observed for the lower band but with peak gain values of about 0 dBic, for both simulations and measurements (all results not reported for brevity)*
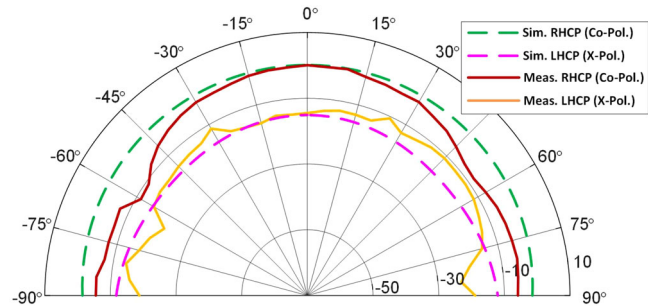

Fig. 9 *Normalized beam pattern for CP1 (RHCP) at the lower band by driving ports 1 to 4. The corresponding cross-polarization level is also shown*
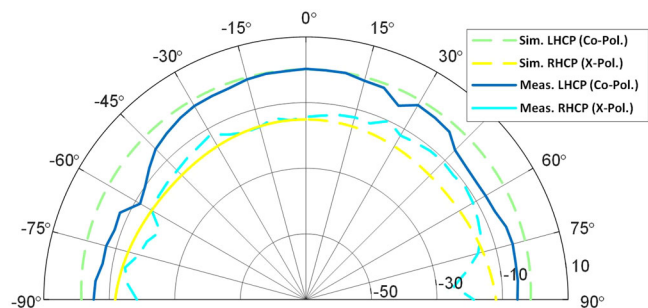

Fig. 10 *Normalized beam pattern for CP2 (LHCP) at the lower band by driving ports 5 to 8. The corresponding cross-polarization level is also shown*

dimensions). The antenna array was then measured and tested in the anechoic chamber within The Scottish Microelectronics Centre at The University of Edinburgh.

Measurement results for the reflection coefficients for both frequency bands are shown in Figures 6 and 7 for element 1. The optimized (or initially designed and then simulated) S_{11} result for the lower operational frequency (which is within the L-band) is less than −10 dB at
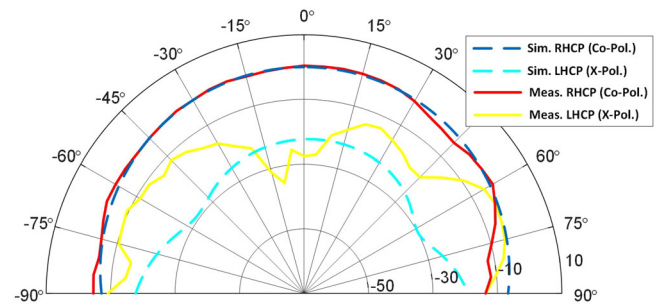

Fig. 11 *Normalized beam pattern for CP1 (RHCP) at the upper band by driving ports 1 to 4. Shown also is the corresponding cross-polarization level*
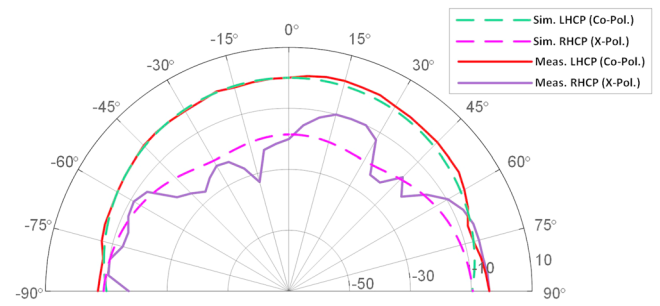

Fig. 12 *Normalized beam pattern for CP2 (LHCP) at the upper band by driving ports 5–8. The corresponding cross-polarization level is also shown*

1.1 GHz, while it is less than −15 dB at 2.4 GHz for the upper band (which is within the S-band) for P1. Similar findings were observed for the remaining ports. However, for the measurements, both sets of reflection coefficients are less than −12 dB at about 1.04 GHz and less than −16 dB at 2.37 GHz for P1. Similarly for P2. This downward shift in frequency is due to practical fabrication tolerances; basically the layer lengths and spacing between the layers had some small offsets from the earlier optimized design of about ±1 mm (in the worst case). To better understand this tolerancing effect on antenna performance, all structure dimensions were re-introduced into the simulator (which is actually more representative of the proof-of-concept demonstrator) and the structure was re-simulated (or simulated again, see results in Figures 6–8) and a better agreement between the simulations and measurements can be observed. An analogous design approach was completed in [8], for the earlier version of the FSP antenna array which had only four ports, was single-band, and offered a single CP operating state; i.e. only RHCP.

When preparing for the CP measurements in the far-field, we needed to generate DCP antenna radiation by applying the appropriate phase shift to ports P1, P2, P3, and P4 for CP1, and similarly, P5 to P8 for CP2. To achieve this feeding we used two external 90° hybrid couplers and one 180° hybrid coupler (similar feeding arrangements were employed in [8] and [24–27]). With this feeding, the measured and simulated realized gain peak versus frequency as well as the beam patterns for both CP1 and CP2 states were recorded for both frequencies, as reported in Figures 8–12.

Both measured and simulation results are generally in agreement. For the lower band, the realized gain maximum was about 0 dBic at 1.1 GHz for the simulations and measurements. While for the upper band, the realized gain maximum was about 2 dBic at 2.3 GHz (see Figure 8), and this is in agreement with the frequency for best matching as shown in Figure 7. These low CP gain values and broadbeam antenna features are generally required for telemetry, satellite positioning in space, and maintaining link coverage over a large angular range as in the M3M [13, 14, 18] and Unicorn [17] satellite missions.

It should also be mentioned that there is a minor beam squint for the measured patterns in the principal planes at about 45° (see Figures 9–12) and this is related to practical challenges when measuring compact antenna structures (similar issues were observed in [8]). Regardless, for the lower band the cross-polarization (x-pol.) level is about 15 dB below the main broadside beam maximum for CP1 and the same for CP2. This

is related to the compactness of the ground plane and antenna itself; i.e. the structure size is only $0.18\lambda \times 0.18\lambda$ at the lower band. However, the x-pol. level is more than 25 dB below the main broadside beam maximum for CP1 and about 18 dB below for CP2 at the upper band (since the structure is electrically larger; $0.40\lambda \times 0.40\lambda$). These findings generally define good polarization purity for both bands, and over an angular range of $\pm 45°$. In addition, the axial ratio (AR) was determined to be less than 3 dB for the lower band and it is less than 1 dB for the higher frequency band over a $40°$ beam angular range.

Conclusion: This letter reported on a 2×2 FSP antenna array by using sequential rotation of four dual-linear polarized elements. For structure compactness, folding and shorting as well as meandering was employed. The proposed antenna has been design and optimized using CST and then fabricated and measured. Simulation and measurement results shows good agreement in terms of reduced reflections, albeit a slight downward shift in the operating frequencies of the antenna and this is due to the noted fabrication tolerances. Applications include simultaneous L-Band and S-band operation on CubeSats, picosatellites as well as other small satellite structures whilst offering DCP functionality. The narrow bandwith of the electrically compact antenna for the lower band may be suitable for low data rate communications [18] and other telemetry and positioning scenarios, which is critical for onboard satellites systems. The upper band can be useful for downlinks [22], connectivity to other satellite constellation networks, and ground station communications.

References

1 Sandau, R.: Status and trends of small satellite missions for earth observation. *Acta Astronaut.* **66**(1–2), 1–12 (2010)

2 Gao, S., et al.: Advanced ants for small satellites. *Proc. IEEE* **106**(3), 391–403 (2018)

3 Heidt, H., et al.: CubeSat: a new generation of picosatellite for education and industry low-cost space experimentation. In: 14th Annual/USU Conference on Small Satellites, pp. 1–19. Utah State University, Logan, UT (2000)

4 Rahmat-Samii, Y., Manohar, V., Kovitz, J.M.: For satellites, think small, dream big: a review of recent antenna developments for cubeSats. *IEEE Antennas Propag. Mag.* **59**(2), 22–30 (2017)

5 Muri, P., Challa, O., McNair, J.: Enhancing small satellite communication through effective antenna system design. In: 2010-Milcom 2010 Military Communications Conference, pp. 347–352. IEEE, Piscataway, NJ (2010)

6 Gao, S., et al.: Antennas for modern small satellites. *IEEE Antennas Propag. Mag.* **51**(4), 40–56 (2009)

7 Chahat, N., et al.: Advanced CubeSat antennas for deep space and earth science missions: a review. *IEEE Antennas Propag. Mag.* **61**(5), 37–46 (2019)

8 Li, Y., Podilchak, S.K., et al.: Compact antenna for picosatellites using a meandered folded-shorted patch array. *IEEE Antennas and Wireless Propag. Lett.* **19**(3), 477–481 (2020)

9 Khan, M.U., Sharawi, M.S., Mittra, R.: Microstrip patch antenna miniaturisation techniques: a review. *IET Micro, Antennas Propag.* **9**(9), 913–922 (2015)

10 Patel, B., Narang, T., Jain, S.: Microstrip patch antenna-a historical perspective of the development. In: Conference on Advances in Communication and Control Systems, pp. 445–449. Atlantis Press, Dordrecht (2013)

11 Garg, R., et al.: *Microstrip Antenna Design Handbook.* Artech House, Norwood, MA (2001)

12 Li, R., et al.: Development and analysis of a folded shorted-patch antenna with reduced size. *IEEE Trans. Antennas Propag.* **52**(2), 555–562 (2004)

13 Podilchak, S.K., et al.: A compact circularly polarized antenna using an array of folded-shorted patches. *IEEE Trans. on Antennas Propag.* **61**(9), 4861–4867 (2013)

14 Podilchak, S., et al.: Compact antenna for microsatellite using folded shorted patches and an integrated feeding network. In: 2012 6th European Conference on Antennas and Propagation (EUCAP), pp. 1819–1823. Prague, Czech Republic (2012)

15 Debogović, T., et al.: Low-profile multi-function antenna system for small satellites. In: 2016 10th European Conf on Antennas Propag. (EuCAP), pp. 1–5. IEEE, Piscataway, NJ (2016)

16 Podilchak, S.K., Murdoch, A.P., Antar, Y.M.M.: Compact, microstrip-based folded-shorted patches: PCB antennas for use on microsatellites. *IEEE Antennas Propag. Mag.* **59**(2), 88–95 (2017)

17 Unicorn-2 satellite platform. http://www.albaorbital.com/. Accessed 20 March 2021

18 Maritime monitoring and messaging microsatellite (M3MSat) mission. https://www.asc-csa.gc.ca/eng/satellites/m3msat/default.asp. Accessed 30 June 2023

19 Zhang, J., Breinbjerg, O.: Miniaturization of multiple-layer folded patch antennas. In: 2009 3rd European Conference on Antennas and Propagation, pp. 3502–3506. (2009)

20 Brocker, D.E., et al.: Miniaturized dual-band folded patch antenna with independent band control utilizing an interdigitated slot loading. *IEEE Trans. Antennas Propag.* **65**(1), 380–384 (2016)

21 Kundu, D., Reza, A.W., Ramiah, H.: Design of an U-slot folded shorted patch antenna for RF energy harvesting. In: 2nd International Conference on Innovations in Engineering and Technology, pp. 61–65. International Institute of Engineers, Kolkata (2014)

22 Buendía, V.G.G., et al.: Compact and planar end-fire antenna for PicoSat and CubeSat platforms to support deployable systems. *IEEE Open J. Antennas Propag.* **3**, 1341–1350 (2022)

23 Alshammari, B., et al.: Dual-band dually-polarized compact folded-shorted patch array for small satellites. In: IEEE International Symposium on Antennas and Propagation and USNC-URSI Radio Science Meeting (APS/URSI), pp. 707–708. (2021)

24 Kuznetcov, M.V., et al.: Planar feeding circuit integrated with a compact dielectric resonator for polarization diversity. *IEEE Trans. Microwave Theory Tech.* **69**(4), 2229–2240 (2021)

25 Kuznetcov, M.V., et al.: Hybrid dielectric resonator antenna for diversity applications with linear or circular polarization. *IEEE Trans. Antennas Propag.* **69**(8), 4457–4465 (2021)

26 Kongpop, U., et al.: A broadband planar magic-T using microstrip-slotline transitions. *IEEE Trans. Microwave Theory Tech.* **56**(1), 172–177 (2008)

27 Brzezina, G., Roy, L.: Miniaturized $180°$ hybrid coupler in LTCC for L-band applications. *IEEE Microwave Wireless Compon. Lett.* **24**(5), 336–338 (2014)